Pseudo-geodesic gridshells

Romain Mesnil, Olivier Baverel

Pseudo-geodesic gridshells

Romain Mesnil[a], Olivier Baverel[a,b]

[a] *Navier, UMR 8205, Ecole des Ponts, Université Gustave Eiffel, CNRS*
[b] *GSA, ENS Architecture de Grenoble*

Abstract

Elastic gridshells are efficient structures covering large spans with little material. They are fabricated using a network of straight members deformed into doubly curved shapes. Researchers and builders have used two families of remarkable curves to generate gridshells with straight planks: geodesic gridshells, where the planks follow the geodesic curves and lay along the tangent plane of the surface, and asymptotic gridshells, where the planks follow asymptotic lines and are orthogonal to the surface normal. This article proposes the concept of pseudo-geodesic gridshells, where planks follow pseudo-geodesic curves of a surface. This article introduces a scaling argument showing that the structural efficiency of pseudo-geodesic gridshells may be twice as much as geodesic gridshells. This is illustrated by a parametric study that implements linear buckling analysis on various pseudo-geodesic gridshells.

Keywords: architectural geometry, gridshell, buckling analysis, performance assessment

1. Introduction

Elastic gridshells are structures composed of a network of beams that are elastically deformed to map a doubly-curved surface. They have been pioneered by Frei Otto in the 1970's, with the Mannheim Multihalle, designed in collaboration with engineers from Ove Arup and Partners, being the culmination of timber elastic gridshells of that era [1]. However, few gridshells have been built since then, with the notable exception of the roofs of the Downland museum

[2] and Savill Building designed by Buro Happold in the early 2000s. Elastic gridshells have since then known a rebirth, with the introduction of novel form-finding techniques, like the formulation of beam elements with dynamic relaxation [3], but also of new materials, such as composite materials (GFRP), which significantly increase the stiffness of elastic gridshells [4, 5].

In parallel, the knowledge of architectural geometry has vastly increased during the last decade. A new point of view on constructive geometry, based on theoretical results on discrete geometries and computational methods from the computer graphics community has paved the way to more flexible design workflows for free-form structures [6]. This paper aims to make a modest contribution that would bridge these two communities by introducing a new family of structures for elastic gridshells, based on pseudo-geodesic lines, a seemingly unexplored family of curves in structural engineering.

1.1. Previous work on constructive geometry of gridshell structures

Frei Otto and the Institute for Lightweight Structures in Stuttgart (ILEK) are the pioneers of elastic gridshells. Their projects rely on Tchebycheff net, a constant-length quadrilateral network with zero-shear stiffness. Such gridshells can be laid flat on the ground and then deformed in a 3D shape with cranes. Tchebycheff nets are the preferred method to construct elastic gridshells nowadays and are still an active topic of research [7, 8].

The main limitation of Tchebycheff nets is that those networks may result in large torsion in members. As such, it is extremely difficult to map a grid structure constituted of laths that would be at equilibrium on an arbitrary shape: the simulation of the coupling between bending and torsion is then necessary to determine whether the construction of elastic gridshell with straight planks is feasible [9].

The late Julius Natterer proposed a different methodology to construct elastic gridshells with timber laths, namely to follow *geodesic curves*. Geodesic curves have a straight flattening property: a lath that follows a geodesic curve and remains tangent to the target surface can be unrolled in a rigorously flat

(a) EPFL Polydome: an example of geodesic gridshell (picture : EPFL-MEDIACOM, distributed under Creative Commons 4.0 License.)

(b) An example of asymptotic gridshell (picture :[10])

Figure 1: Examples of gridshells constructed with straight planks.

and straight strip. The largest timber gridshell built using this technique seems to be the EXPO Dach in Hannover [11]. The Polydome at EPFL, shown in Figure 1a is also a significant example of this construction technique. Due to their simplicity of assembly, geodesic gridshells have been the subject of small research pavilions [12, 13]. The main limitation of geodesic gridshell is that laths are laid tangentially on the surface and the resulting structure has limited bending stiffness. It is then necessary to stack laths and bind them by nailing them, which is the technological solution for the previous examples. Furthermore, it shows that it is rather difficult to build a geodesic gridshell from a flat configuration.

More recently, Schling *et al.* [14] proposed to use asymptotic lines to construct elastic gridshells. Asymptotic lines have zero normal curvature so that a lath following an asymptotic line and remaining perpendicular to the surface can be unrolled in a straight manner. The main limitation of asymptotic lines is that they only exist on surfaces with negative Gaussian curvature. An example of an asymptotic gridshell is shown in Figure 1b: despite the geometrical complexity, all steel strips are rigorously straight upon unrolling.

It will be shown in the second section of this article that the two seemingly independent design approaches of Natterer and Schling may be unified through the definition of pseudo-geodesic curves. The main objective of this unifying

approach is to circumvent the limitations of both methods, namely to benefit from a significant bending stiffness while being able to map positively curved surfaces.

1.2. Previous work on the structural design of elastic gridshells

This section aims now at introducing relevant background on the design of elastic gridshells. Detailed design issues are left aside, and the emphasis is set on simple scaling arguments on gridshell buckling.

Due to their slenderness, the design of gridshell is often governed by potential instabilities, a topic that has been studied by Victor Gioncu in the early 1990s [15]. A collaborative research effort from the Working Group on Metal Spatial Structures of the International Association for Shell and Spatial Structures led to guidelines in 2012 [16]. Eurocode 3 states that linear buckling analysis may be used, but that the buckling factor should exceed 10, which is considered too conservative, and nonlinear analysis is preferred in practical applications. Gridshells are sensitive to geometrical and material imperfections, as initially shown in [17] and more recently in [18]. It has been shown in two studies that the pre-stress of elastic gridshells has little influence on their buckling load [19, 20], while a robustness study illustrates the low reserve of post-buckling resistance, due to the redistribution of the pre-stress after buckling [21]. The same study showed that for a gridshell with few openings, the stress at buckling failure was ten times less than the pre-stress due to the elastic bending of rods, and remained far below the material failure criterion. A recent study with numerical and experimental results comes to a similar conclusion for geodesic gridshell [22]. Therefore, the initial buckling load is the main quantity of interest in the study of elastic gridshells.

Equivalent continuum models for buckling load of gridshells have been proposed in previous literature [23, 24]. The equivalent bending stiffness $\mathcal{D}$ depends on the grid topology (triangular, quadrangular, tri-hex, etc.) [25], orientation [26], and may depend non-linearly on the grid subdivision. In practice, elastic gridshells are two-way grids with almost zero membrane shear stiffness, to allow

a change in Gaussian curvature. Bracing is added, either through rigid bracing [27], cables or a third layer of bent elastic rods [28], to fully benefit from a shell-like behaviour. In the case of a properly braced structure, the critical pressure scales as in equation (1), as proposed by Malek *et al.* [23] following a series of previous work on equivalent continuum models for gridshells [29] and analytical thin-shell buckling formulae for spherical caps. It should be recalled however that this equation is only valid for global buckling mode, and that gridshell structures are subject to other instabilities, like nodal snap-through, or lateral-torsional buckling of a single member [17]. This scaling equation, although useful for preliminary design, does not replace a nonlinear analysis of the gridshell with imperfections, which is the only way to capture the local buckling modes and potential interaction between buckling modes. The critical buckling pressure proposed by [23] reads as follows:

$$p \propto \frac{\sqrt{\mathcal{A}\mathcal{D}}}{R^2} \tag{1}$$

Where $\mathcal{A} = ES/l$ and $\mathcal{D} = EI/l$ are homogenised membrane and bending stiffness and the scaling factor depends on the geometry and pattern [30, 31]. With rectangular cross-section of width b and height h, $\mathcal{A} = Ebh/l$ and $\mathcal{D} = Ebh^3/(12l)$. The *structural efficiency* may be defined as the ratio between critical buckling pressure and surface weight. This notion has already been used in [23] and [24]. Since the surface weight is proportional to S/l, the structural efficiency Π^* is thus

$$\Pi^* \propto \frac{E}{R^2} \cdot \sqrt{\frac{I}{S}} \tag{2}$$

The simple formula for critical pressure shows that curvature positively and greatly impacts the buckling capacity of gridshell structures. The application of the formula for a beam of height h and width b also shows that structural efficiency scales with h, and thus that an increase in beam height results in more efficient structures. However, in elastic gridshells, a compromise between curvature and member stiffness must be met. Indeed, the Euler-Bernoulli model gives a relation between the maximal bending stress σ_{max}, Young modulus E,

the beam curvature κ and the height of the beam in the bending direction h.

$$\sigma_{max} = \frac{Eh\kappa}{2} \tag{3}$$

For a given material, the design stress for long-term bending σ_d and Young modulus E are known. For a given targeted curvature, we may thus deduce the maximal height of the beam:

$$h < \frac{2\sigma_d}{E\kappa} \tag{4}$$

Therefore, the structural efficiency of elastic gridshells is limited by the shaping process, which restricts the maximal dimensions of its members.

1.3. Problem statement

This article aims to unify the geometrical approach of Natterer and Schling by proposing the concept of pseudo-geodesic gridshells. We will show the fundamental geometrical properties of these objects, and discuss the potential benefit in terms of structural performance. Simplified guidelines will be proposed to optimise the performance of pseudo-geodesic gridshells.

The second section recalls the definition of pseudo-geodesic curves and implications for construction. The third section discusses some scaling considerations regarding their efficiency. The fourth section proposes a numerical parametric study of pseudo-geodesic gridshells on a toroidal cap with positive Gaussian curvature. We conclude this paper with a discussion on the potential of pseudo-geodesic gridshells as lightweight structures based on the numerical evidence gathered in this study.

2. Geometrical properties of pseudo-geodesic networks

2.1. Curves on surfaces

Elastic gridshells are constituted of slender members: their geometry lends thus itself to the study of curves (the neutral axes of the gridshells) drawn on a surface (understood as the mid surface of the equivalent shell). This subsection

aims at providing a brief overview of this topic for the reader and recalls the mathematical definition of pseudo-geodesic curves.

While structural engineers may be used to work with Frenet-Serret frame $(\mathbf{t}, \mathbf{N}, \mathbf{B})$, which is convenient for computing stresses, this frame does not capture any information on an embedding surface. This limitation has led to the introduction of the Darboux frame. It is defined as follows and is illustrated in Figure 2.

- $\mathbf{t}$ is the tangent vector of the curve;
- $\mathbf{n}$ is the surface normal;
- $\mathbf{g} = \mathbf{t} \wedge \mathbf{n}$ is the tangent normal vector.

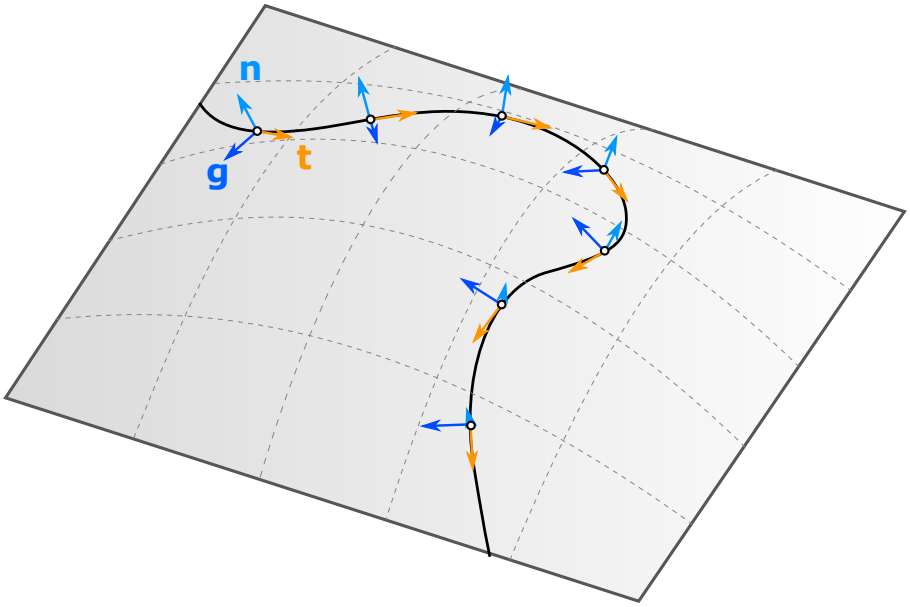

Figure 2: Darboux frame of a curve embedded on a surface.

The Darboux frame allows to define three new curvatures:

- $\kappa_n = \frac{\mathrm{d}\mathbf{t}}{\mathrm{d}s} \cdot \mathbf{n}$ is the normal curvature.
- $\kappa_g = \frac{\mathrm{d}\mathbf{t}}{\mathrm{d}s} \cdot \mathbf{g}$ is the geodesic curvature.

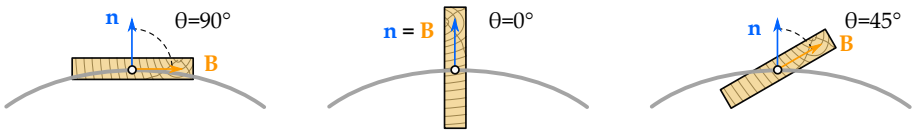

Figure 3: Visualisation of material frame in pseudogeodesic curve gridshells in the plane perpendicular to $\mathbf{t}$. From left to right: plank laid along a geodesic, asymptotic gridshell, and a 45° pseudo-geodesic curve.

- $\tau_g = \frac{\mathrm{d}\mathbf{n}}{\mathrm{d}s} \cdot \mathbf{g}$ is the geodesic torsion.

The normal curvature is the projection of the curvature vector $\kappa\mathbf{N}$ in the $(\mathbf{t}, \mathbf{n})$ plane, while the geodesic curvature is the projection of the curvature vector in the osculating plane. It follows that $\kappa_g^2 + \kappa_n^2 = \kappa^2$. Writing θ the angle between $\mathbf{n}$ and $\mathbf{N}$, we have a more compact formula, sometimes referred to as *Meusnier theorem*.

$$\begin{cases} \kappa_n = \kappa \sin\theta \\ \kappa_g = \kappa \cos\theta \end{cases} \tag{5}$$

Normal curvature plays an important role in differential geometry. It is well-known that, at any point, two directions respectively minimise and maximise normal curvature. They are called principal curvature directions, and we write κ_1 and κ_2 the maximal values of normal curvature. By convention, we have $\kappa_1 > \kappa_2$. It is then possible to define Gaussian and mean curvature as follows:

$$\begin{cases} K = & \kappa_1 \cdot \kappa_2 \\ H = & \frac{1}{2} \cdot (\kappa_1 + \kappa_2) \end{cases} \tag{6}$$

2.2. Basic geometry of pseudo-geodesic curves

Pseudo-geodesic curves have first been studied by Wunderlich [32]. A series of equivalent definitions of pseudo-geodesic curves can be found in the literature.

Definition 1. *pseudo-geodesic curves* are curves traced on surfaces so that the angle between the curve binormal $\mathbf{B}$ and the surface normal $\mathbf{n}$, written θ in the followings of this article, is a constant.

Definition 2. Pseudo-geodesic curves are such that the ratio between normal curvature and total curvature is constant.

Proof of equivalence:. Definitions 1 and 2 are equivalent by direct application of equation (5). The ratio is constant and equal to $\sin\theta$.

The reader should by now be familiar with the two limit cases of pseudo-geodesic curves, shown in Figure 3.

- The case $\theta = \pi$ corresponds to geodesics (left of Figure 3).
- The case $\theta = 0$ corresponds to asymptotic curves, which exist only on anticlastic surfaces (middle of Figure 3).

It shall be noticed that pseudo-geodesics create a one-parameter interpolation between the two extreme scenarios: this is why the authors consider it to be the generalization of both geodesics and asymptotic lines. Some properties of pseudo-geodesics have been used in the context of pleated structures in [33]. Pseudo-geodesics all benefit from the *straight-flattening property*. First, the strip generated from the ruling direction emerging from the binormal vector of a curve $\mathbf{B}$ has a rigorously straight development. Second, by *Definition 1* these directions happen to make a constant angle θ with the normal, which greatly simplifies the fabrication of connectors.

2.3. Pseudo-geodesic gridshells

Definition 3. Pseudo-geodesic gridshells are gridshells which are constructed from a network of beams, whose neutral axis is following pseudo-geodesic curves of a surface.

Pseudo-geodesics may guarantee a high node congruence, a topic of interest in gridshell manufacturing [34]. The key fact is that, by definition, the osculating plane $(\mathbf{T}, \mathbf{N})$ of a pseudo-geodesic has a constant angle with the osculating plane of the surface, as shown in Figure 3. Conversely, the surface normal also has a constant angle with the plane $(\mathbf{T}, \mathbf{B})$ of the pseudo-geodesic curve. Figure 4 illustrate a potential concept of connection detail. The blue axis is aligned with

the surface normal: the two wedges can rotate freely around the blue axis to accommodate the angle between two pseudo-geodesic curves. The wedges have a constant angle because they are aligned with the surface normal on one side and the binormal vector of the pseudo-geodesic curve on the other side. Figure

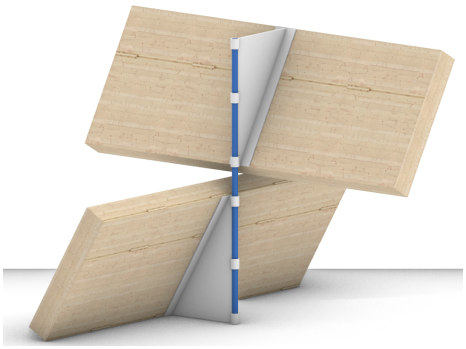

Figure 4: A node in a pseudo-geodesic gridshell. The blue axis is aligned with the surface normal, the grey parts are free to rotate along the axis. The wedge angle is constant.

5 shows a negatively curved surface mapped with a pseudo-geodesic gridshell. The angle θ is equal to 45°, which is an intermediate configuration between asymptotic lines and geodesic lines.

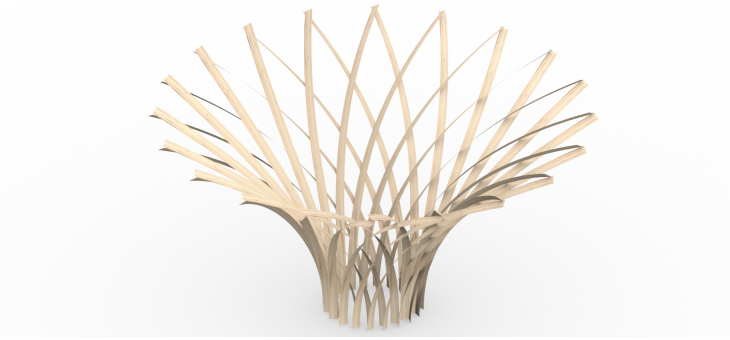

Figure 5: A pseudo-geodesic-gridshell with $\theta = 45°$ on a negatively-curved surface.

2.4. Local existence of pseudo-geodesic curves

So far, it seems that existence of pseudo-geodesic curves on surfaces is only proven locally but their global behaviour has not been thoroughly studied. The

local existence can be determined thanks to red Euler's formula for normal curvature, given by equation (7).

$$\kappa_n = \kappa_1 \cos^2 \phi + \kappa_2 \sin^2 \phi \tag{7}$$

This equation links the normal curvature κ_n of a curve making an angle ϕ with the first principal direction at a point of a surface with principal curvatures κ_1 and κ_2. Figure 6 represents the relation between curvature and the orientation of a curve with respect to the first principal curvature direction. The angle ϕ corresponds to the angle between the tangent vector of a curve and the first principal curvature direction.

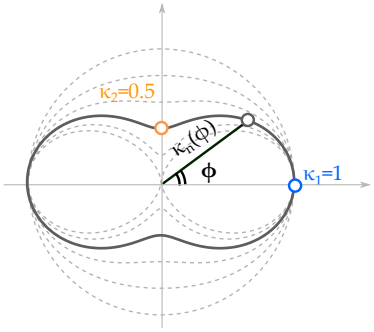

Figure 6: Visualisation of Euler formula for normal curvature in polar coordinates in the κ_1,κ_2 space.

This formal equation linking curvature and orientation is recalled in equation (7). There is one solution for ϕ, except for $\theta = 0$, and thus the local existence of a pseudo-geodesic curve is always guaranteed, except for asymptotic curves, which only exist when Gaussian curvature is negative.

2.5. Global existence of pseudo-geodesic curve

The local existence of pseudo-geodesics is guaranteed by equation (7), except in the case of asymptotic lines on positively curved surfaces. However, one might be interested in the properties of pseudo-geodesic curves on arbitrary surfaces. This paragraph discusses the intrinsic limitations of pseudo-geodesic curves by introducing an upper bound on the total area of curvature enclosed by

pseudo-geodesic lines (grey area in Figure 7). The comparison of curvature of pseudo-geodesic in positive and negative Gaussian curvature regions illustrates significant differences. Let us now consider a closed pseudo-geodesic line as

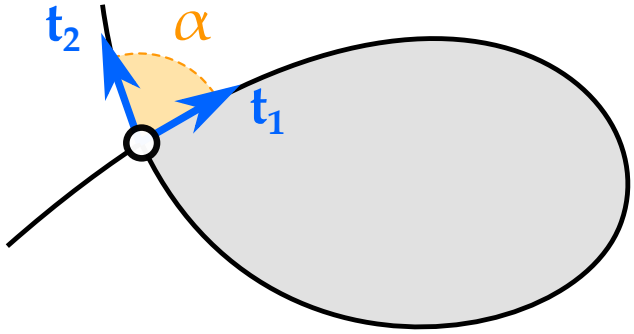

Figure 7: A closed pseudo-geodesic curve. The enclosed region is represented in light grey.

shown in Figure 7. Gauss-Bonnet Formula can be used to relate the integral of Gaussian curvature K to the geodesic curvature of a pseudo-geodesic with a closing angle of α. Meusnier equation (equation (5)) can be used to substitute curve curvature for geodesic curvature.

$$\int_S K \mathrm{d}S + \cos\,\theta \cdot \int_\Gamma \kappa\,(s)\ \ \mathrm{d}s + \alpha = 2\pi\chi \tag{8}$$

The integral of curvature (also called *total curvature*) is a quantity superior to 2π, with equality only for plane curves with a turning number of 1. This gives an upper bound to the integral of Gaussian curvature bounded by a closed smooth pseudo-geodesic. This upper bound is reached for planar pseudo-geodesics with a turning number of 1.

$$\int_S K \mathrm{d}S \leq 2\pi\,(\chi - \cos\,\theta) - \alpha \tag{9}$$

The right-hand side is a decreasing function of θ. If we restrict our study to bounded surfaces homotopic to a disk ($\chi = 1$), which is a reasonable assumption for elastic gridshells, then we see that the integral of the right-hand-side becomes 0 for $\theta = 0$ and $\alpha = 0$, which is the trend observed on the sphere. Notice that no limitation appears for negatively curved surfaces, since the derivation of the Gauss-Bonnet formula yields an upper bound.

2.6. Curvature of pseudo-geodesics

Another point of view on the practical limitations of pseudo-geodesics on surfaces is the study of their curvature. Euler formula and Meusnier theorem yield a remarkable equality for pseudo-geodesic curves:

$$\kappa = \frac{\kappa_1 \cos^2 \phi + \kappa_2 \sin^2 \phi}{\sin \theta} \tag{10}$$

Upper and lower bounds can be constructed for positively curved surfaces ($\kappa_1 \kappa_2 > 0$). Equation (11) sums up these bounds when $|\kappa_1| > |\kappa_2|$.

$$\frac{|\kappa_1|}{\sin \theta} > |\kappa| > \frac{|\kappa_2|}{\sin \theta} \tag{11}$$

Therefore, the closer θ gets to 0 in positively curved regions, the higher the curvature. The lower bound does not exist in negatively curved surfaces since the numerator in equation (10) can be zero. This fact is well illustrated by doubly ruled surfaces since ruling directions are asymptotic directions ($\kappa = 0$, $\theta = 0°$).

3. Analytical considerations on the mechanical performance of pseudo-geodesic gridshells

The previous section has introduced pseudo-geodesic gridshells and some key geometrical properties. This section is devoted to the comparison of relative performance between conventional geodesic gridshells with pseudo-geodesic gridshells.

3.1. Bending stiffness

Although geodesic gridshells are easily constructed, they suffer from a low bending stiffness. Indeed, the restrictions on beam height set in equation (4) impose a limitation of bending stiffness, and thus of critical buckling pressure.

Pseudo-geodesic gridshells offer the potential to circumvent this limitation. Indeed, the bending I stiffness of a lath of with b and height h, whose strong axis is inclined at an angle θ with the surface normal is given in equation(12).

$$I = \frac{hb^3}{12}\cos^2\theta + \frac{bh^3}{12}\sin^2\theta \tag{12}$$

Figure 8 shows the ratio between $I(\theta)$ and $I(0)$ for different ratios between b and h. The derivative $\mathrm{d}I/\mathrm{d}\theta$ is 0 for $\theta = 0$ and $\theta = 90°$, which means that small changes compared to asymptotic curves lead to a marginal decrease of bending stiffness. The graph also shows that geodesic gridshells have comparatively lower bending stiffness than asymptotic gridshells.

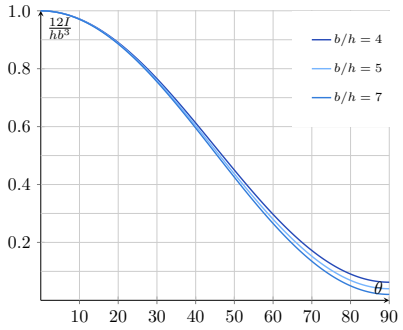

Figure 8: Evolution of dimensionless bending stiffness with respect to θ. $\theta = 0°$ corresponds to asymptotic gridshells while $\theta = 90°$ corresponds to geodesic gridshells.

The relative structural efficiency of pseudo-geodesic gridshells can be estimated with (13), which combines equations (2) and (12).

$$\frac{\Pi^*}{\Pi^*_{geodesic}} \sim \sqrt{\frac{12I}{S}} \tag{13}$$

The graph of this function is shown in Figure 9. It hints that the inclination of members should result in more efficient structures. For example, with a lath with a ratio $b/h = 7$, an angle $\theta = 65°$ yields a 3-folds improvement of structural efficiency if the same cross-section is used.

3.2. Accounting member curvature in positively curved areas

Section 2.6 has highlighted intrinsic curvature limitation for pseudo-geodesic curves in positively-curved gridshells. It has been shown that $\kappa > k_{min} \cdot \kappa_2$, where $k_{min} = 1/\sin\theta$ is shown in Figure 10. An upper bound on maximal

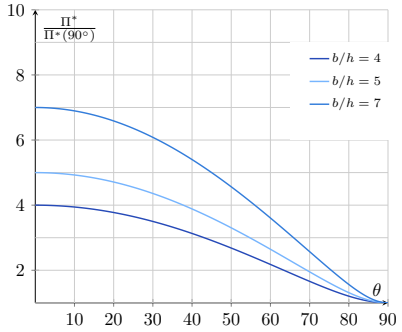

Figure 9: Structural efficiency normalised with respect to the structural efficiency of geodesic gridshells for structures with the same cross-section..

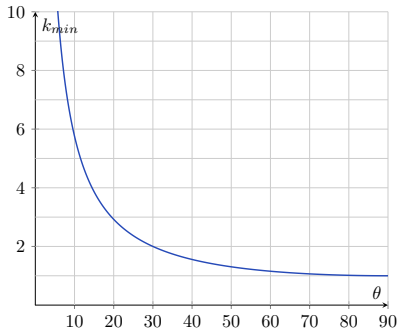

Figure 10: Evolution of curvature amplification factor in positive Gaussian curvature k_{min} with respect to θ

lath height results from equation (4) and is written in equation (14). In this equation the first term of the right-hand side depends on material only, the second depends on shape only, while the third term $\sin\theta$ only depends on the pseudo-geodesic angle.

$$h_{max} = \frac{2\sigma_d}{E} \cdot \kappa_2 \cdot \sin\theta \tag{14}$$

The structural efficiency taking into account the constraint on maximal member height is expected to follow the following equation:

$$\frac{\Pi^*_{constrained}}{\Pi^*_{constrained,90°}} = \sin\theta \sqrt{\sin^2\theta + \frac{b^2}{h^2}\cos^2\theta} \tag{15}$$

The plot of equation (15) is shown in Figure 11. It can be seen that the efficiency

converges to zero for $\theta \to 0$ and that a maximum is reached for $\theta \sim 45°$. More precisely, a simple derivation of equation (15) with respect to θ shows that the minimum is reached for $\theta = \theta_{opt}$:

$$\theta_{opt} = \text{atan}\sqrt{\frac{1}{1 - \frac{2h^2}{b^2}}} \tag{16}$$

The value of θ_{opt} converges to $\theta \sim 45°$ when the ratio b/h becomes large, which is the case of interest in pseudo-geodesic gridshells. In the end, a simplified value of the optimal relative efficiency is found by using the approximation $\theta_{opt} \sim 45°$:

$$\max\left(\frac{\Pi^*_{constrained}}{\Pi^*_{constrained,90°}}\right) \sim 0.5\sqrt{1 + \frac{b^2}{h^2}} \tag{17}$$

The ratio determined in equation (17) corresponds thus to the limits of structural efficiency of pseudo-geodesic gridshells in positively-curved surfaces, as local failure mode may occur before the global failure described by equation (1).

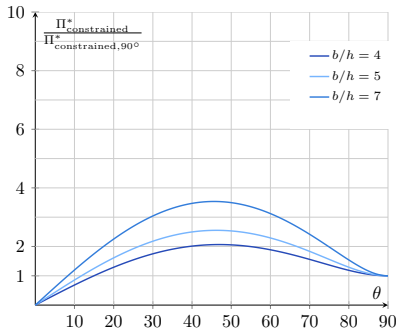

Figure 11: Relative structural efficiency of pseudo-geodesic gridshells on positive Gaussian curvature normalised with the efficiency of a geodesic gridshell. This takes into account the limit curvature of members in pseudo-geodesic gridshells.

4. Mechanical performance of pseudo-geodesic gridshells

The previous sections have introduced pseudo-geodesic gridshells and some analytical considerations on their efficiency. In this section, we investigate the

structural performance of pseudo-geodesic gridshells by performing linear buckling analysis on various gridshells. The goal is to highlight the influence of the inclination of laths on the overall performance. Thus, a simple parametric study is conducted.

4.1. Geometry

Since the previous sections of this article highlight potential limitations in positively curved areas, we generate a portion of torus with positive Gaussian curvature, as shown in Figure 12: the axis of revolution is in the (XY) plane. The torus is then split with a plane parallel to (XY) and offset by L.

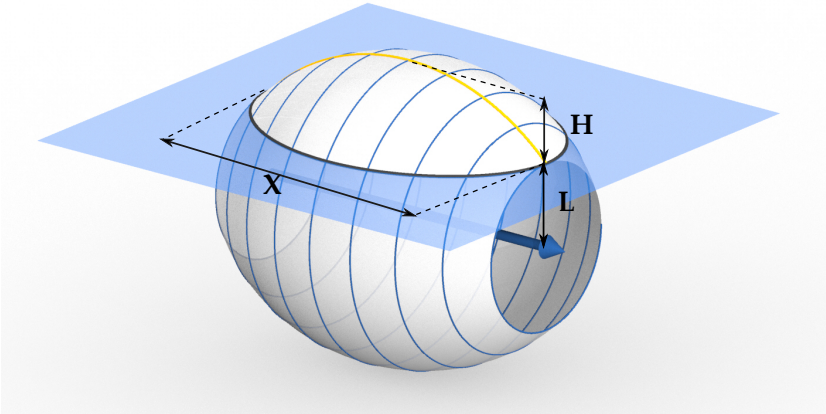

Figure 12: Generation of a portion of a torus

For the sake of conciseness, only one shape is considered. Other studies have thoroughly discussed the influence of shape on the mechanical performance of gridshells [23, 24, 20]. The shape parameters are summed up in eq. (18). The rise-over-span ratio $H/X = 1/7$ is comparable to other gridshells [35].

$$\begin{cases} H = 1m \\ L = 5m \\ X = 7m \end{cases} \tag{18}$$

4.2. Bracing

Gridshell should be braced to fully benefit from their curvature and membrane stiffness [4, 35]. Therefore, the mechanical study should consider a bracing strategy. Several alternatives exist for bracing elastic gridshells.

- Use cables, like for the Mannheim Multihalle [1]. The main disadvantage of this solution is that the pre-stress may be affected by creep-induced deformations of the structure, which requires re-tensioning during the first years.
- Use rigid panels, which requires a geometrical strategy that guarantees planarity of panels, as proposed in [8].
- Use a third layer of elastically bent rods, like in [28]. Although technologically sound, it turns out that the rod's axial stiffness depends on the curvature and spacing of the rods. Details on this aspect can be found in [36].
- Use a third layer of rigid members like done in [37, 27].
- Use moment rigid connections. This is generally not sufficient on its own [4], but this solution can be combined with other bracing strategies. This was used in the Downland Museum gridshell [2], with a patented connection detail.

In this study, we chose to both rigid connections and rigid members, with 50% of the axial stiffness of the laths, and model the rods as truss elements, i.e., they do not contribute to the bending stiffness of the gridshell. Figure 13 shows a possible technological solution for the construction of rigid rod, published by d'Amico *et al.* [27]. So-called *sticks* are attached to the node axis (which in pseudo-geodesic gridshell conicides with the surface normal). The rigid *diagonals* are then overlapped over the sticks and fixed with screws.

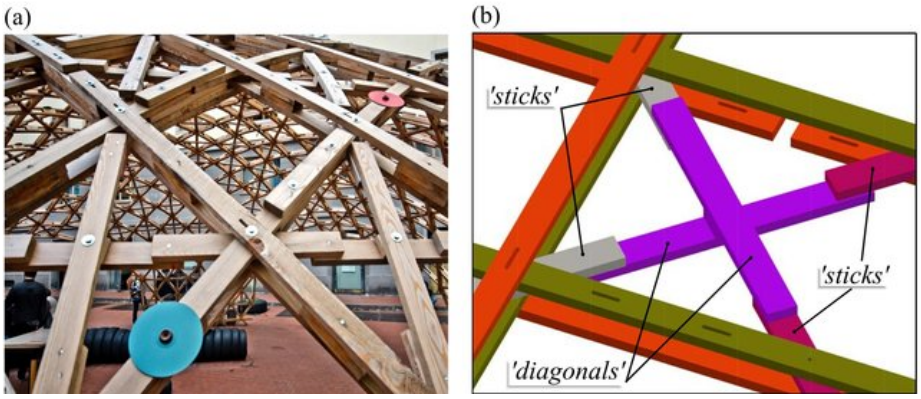

Figure 13: Possible configuration for rigid joints in an elastic gridshell (photo: [27])

4.3. Parametric study

The parametric study consists in generating pseudo-geodesic gridshells on the portion of torus described in Section 4.1. The network of pseudo-geodesic is constructed by generating a single pseudo-geodesic curve, and then by rotating it at an angle π/n. The method used to generate is detailed in the appendix. The parameters to generate a grid are the following:

- The angle θ
- The angle ϕ made by the pseudo-geodesic with the smallest parallel.
- The angle π/n

There are two cross-section parameters for the rectangular profile.

- The beam thickness t
- The beam width b

The parameters n and ϕ were selected so that the average length remains constant while reducing inter-nodal length variations. The maximal length remains thus limited, which avoids lateral-torsional buckling. This selection of parameters reduces the number of parameters in the study.The beam thickness was arbitrarily chosen as 2 centimetres.

Quantity	Values
θ	90, 85, 80, 75, 70, 65, 60
l	0.35 m
b/t	$5, 7$

Table 1: Parameters used in the study.

Figure 14 shows some possible configurations of pseudo-geodesic gridshells. It can be noticed that for the gridshells with $\theta \neq 90°$, the member length l is longer at the bottom of the image. The smaller θ, the more pronounced the phenomenon. It was possible to make a rather even grid spacing with geodesic curves. Interestingly, although the shape has a plane of symmetry in addition to its symmetry of revolution, it is not possible to make a smooth symmetrical grid structure with a pseudo-geodesic gridshell.

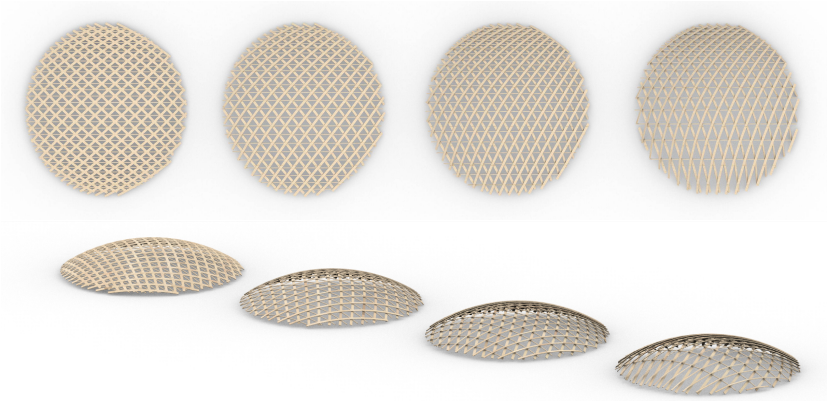

Figure 14: Pseudo-geodesic gridshells with, from left to right, $\theta = 90°$, $80°$, $70°$, $60°$. Notice that the variability of length increases as θ decreases.

Figure 15 illustrates the length variation for different values Φ and θ, where the average length is set to 35cm. It can be seen that the maximal length is, as expected, a decreasing function of θ. For the particular shape treated in this article, the maximal member length becomes more than twice the average member length for $\theta < 65°$. The notion of average member length used in the

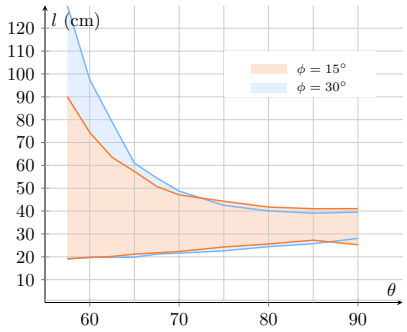

Figure 15: Length variation for two values of Φ. Thick lines represent the minimal and maximal length in the grid.

scaling study becomes then dubious.

4.4. Loads

A non-symmetrical global load pointing downwards is applied to the whole structure according to the pattern shown in Figure 16. Non-symmetrical loads are known to be more critical for the buckling of gridshells, but self-weight may be an important load case in practice, especially because materials used in elastic gridshells are subject to creep and must be designed with a reduced stiffness for those load cases (the k_{def} factor in Eurocode 5 for example). In the followings, p_{cr} refers to the magnitude of the smallest load shown in Figure 16.

4.5. Finite Element Analysis

The structural performance is assessed by performing a linear buckling analysis. The Finite Element software use in this study is Karamba3D. This software is integrated within the visual programming environment Grasshopper [38]. The material used is wood with $E = 10.5GPa$, $G_{12} = 3.6GPa$, $G_3 = 3.6GPa$, $\rho = 6kN/m^3$. The laths are simply supported (no translation allowed at their extremities). The loads are applied as a mesh load, and automatically transfered as line loads to the beams.

The result of linear buckling analysis should be taken with caution because it tends to overestimate the load-bearing capacity of gridshells. Furthermore, it is

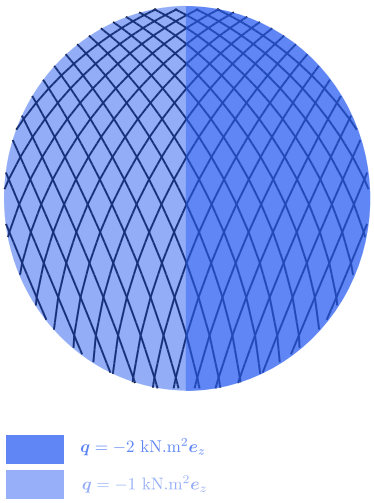

Figure 16: Applied load pattern, seen from top.

necessary to take imperfections into account in detailed design phases. Gioncu and Balut have shown that geometrical imperfections tend to be more critical than material imperfection for large-span slender gridshells [15]. In this study, the neutral axes of the beams are offset due to the geometrical configuration of the laths. This offset is shown in Figure 17, where the thick coloured lines correspond to the geometrical lines used to define the geometry, and dashed lines represent the true position of the beam centroids. It can be noticed in the figure that the eccentricity is equal to $b/2$, which corresponds to at least 5 centimeters for the laths considered in this study. The eccentricities are generated when constructing the beam elements based on information on binormal vector of the beam.

Lefevre *et al.* have studied gridshells with offset resulting from nodal eccentricity and have shown that the offset has the same behaviour as a geometrical imperfection [19]. Therefore, we restrict our study to the structure with the offset.

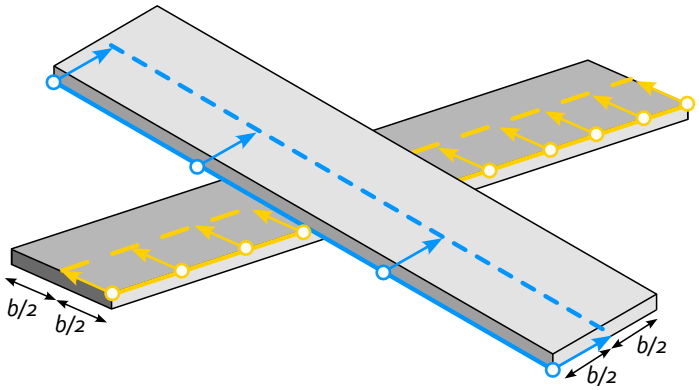

Figure 17: Eccentricity in the finite element model: thick coloured lines correspond to the geometry used for constructing the beams while dashed lines correspond to the true centroid of beams.

4.6. Results

Tables 2 and 3 sum up the results of the parametric study. The result trends are analysed in two graphs shown in Figure 18 and 19.

θ	90	85	80	75	70	67.5	65	62.5	60
ϕ	30	30	30	30	30	15	15	15	15
n	66	72	77	82	86	89	90	94	95
Mass [kg]	514	513	513	513	512	512	512	516	511
p_{cr} [kPa]	12.3	14.9	20.4	25.5	29.0	31.	32.1	33.0	19.1
$\frac{\Pi^*}{\Pi^*_{90}}$	1.0	1.21	1.66	2.07	2.36	2.53	2.61	2.67	1.57

Table 2: Results of the linear buckling analysis calculation for $b/h = 7$.

Figure 18 shows the relative structural efficiency for $b/h = 7$. Here, a constant lath height $h = 2$cm has been considered. For high values of θ, the structure is subject to a global buckling mode and the scaling equation from equation (2) is appropriate. However, for $\theta = 65°$ and below, the first buckling mode corresponds to lateral torsional buckling. As shown in Figure 15, the maximal member length increases as θ decreases, so local buckling is more and

θ	90	85	80	75	70	67.5	65	62.5	60	57.5
ϕ	30	30	30	30	15	15	15	15	15	15
n	66	72	75	82	74	76	78	82	84	86
Mass [kg]	367	364	352	363	360	358	358	365	360	360
p_{cr} [kPa]	8.0	9.8	11.4	13.1	14.9	16.4	17.4	17.9	13.7	6.0
$\frac{\Pi^*}{\Pi^*_{90}}$	1	1.24	1.48	1.65	1.89	2.10	2.23	2.25	1.73	0.76

Table 3: Results of the linear buckling analysis calculation for $b/h = 5$.

more likely to occur.

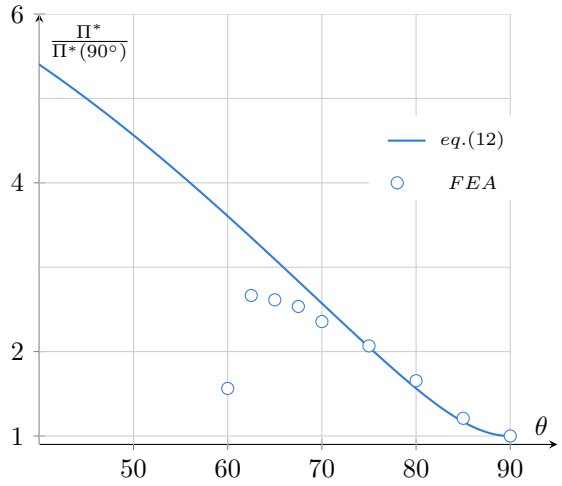

Figure 18: Relative structural efficiency for $b/h = 7$, $h = 2$cm

Figure 19 shows the relative structural efficiency for $b/h = 5$. The same trend can be observed: the finite element analysis is in good agreement with the curve obtained from equation (2) for values of θ above 65°. The relative efficiency of pseudo-geodesic gridshell is multiplied by 2.5 for $\theta = 65°$.

Figure 20 shows the shape associated with the first buckling mode. The transition from a global buckling mode ($\theta = 85°$) to a hybrid buckling mode with nodal snap-through ($\theta = 80°$) and finally to lateral torsional buckling

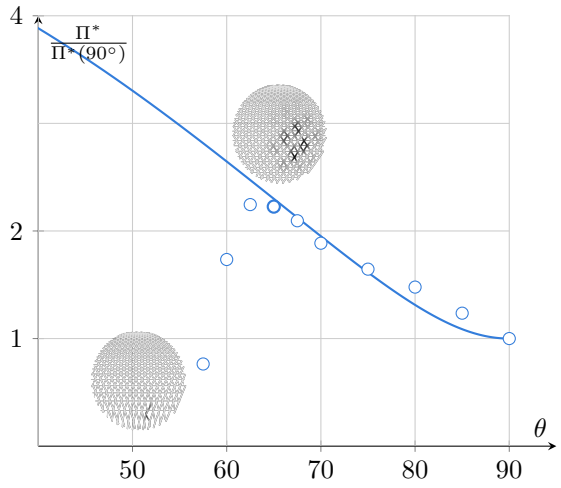

Figure 19: Relative structural efficiency for $b/h = 5$, $h = 2$cm. Buckling pattern is shown for thicker dots.

$(\theta = 62.5°)$ is visible.

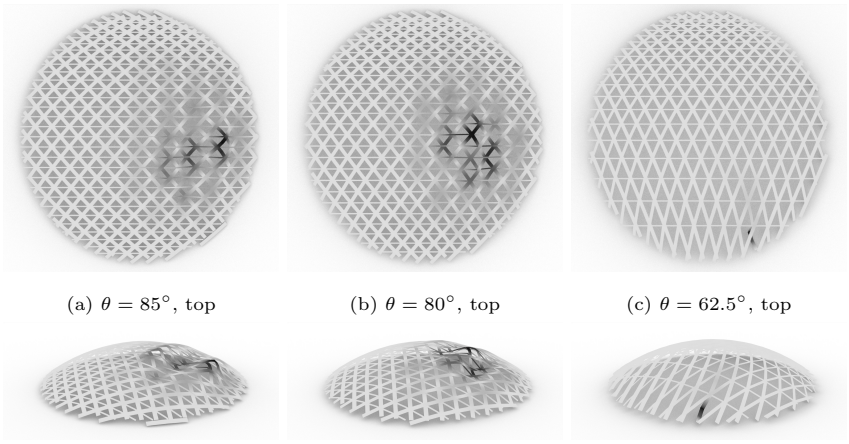

(a) $\theta = 85°$, top (b) $\theta = 80°$, top (c) $\theta = 62.5°$, top

(d) $\theta = 85°$, perspective (e) $\theta = 80°$, perspective (f) $\theta = 62.5°$, perspective

Figure 20: Shape of the first buckling mode for $b/h = 5$ (darker shade indicate larger displacement).

345

4.7. Design guidelines

Pseudo-geodesic gridshells seem to offer a promising alternative to geodesic gridshells, as the structural efficiency and load-bearing capacity increase for low values of θ. The finite element analysis shows a good correlation with the analytical formula derived from previous work [23].

However, pseudo-geodesic gridshells are subject to some limitations in positively curved areas. The maximal length decreases with θ, and the combination of this fact with the inclination of members makes them sensitive to a failure by lateral-torsional buckling of a single member. Therefore, appropriate constructive solutions that restrict lateral-torsional buckling, like the connection of beams to rigid panels, could be envisioned.

Finally, the limitations highlighted in this paper only concern positively curved areas. It is now well-known that asymptotic gridshells can yield aesthetically pleasing curve networks without any limitation on curvature. Negatively curved surfaces or surfaces with both positive and negative curvature are thus a natural application of pseudo-geodesic gridshells.

5. Conclusion

This article has introduced the concept of pseudo-geodesic gridshell, as a generalisation of asymptotic and geodesic gridshells. The geometric principle has been detailed and explains why pseudo-geodesic gridshells may be constructed with a single node and laths with a straight development. Unlike asymptotic gridshells, pseudo-geodesic gridshells may be constructed on surfaces with positive Gaussian curvature, extending thus the formal potential of gridshells built with straight strips. Figure 21 shows three configurations for the same shape.

A lower bound for the curvature of pseudo-geodesic curves on positively curved surfaces has been proposed, and an upper bound for the integral of Gaussian curvature mapped with pseudo-geodesic curves has been derived from the Gauss-Bonnet formula. These two considerations give simple guidelines for mapping pseudo-geodesic curves on complex shapes. Information on the

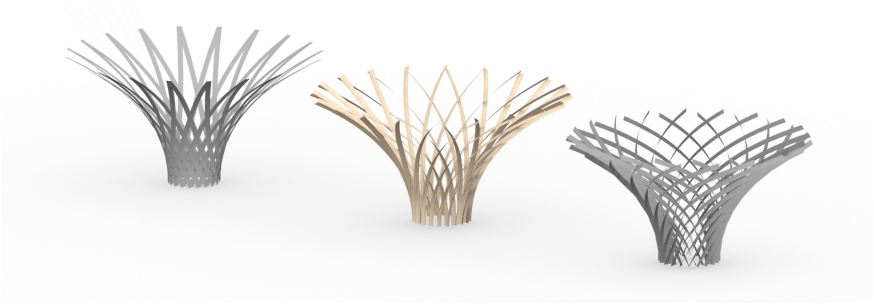

Figure 21: From left-to-right: geodesic gridshell, pseudo-geodesic gridshell and asymptotic gridshell.

maximal normal curvature and integral of positive Gaussian curvature provide necessary conditions for the construction of pseudo-geodesic gridshells.

Simple estimations of the relative efficiency of pseudo-geodesic gridshells have been made. This estimation leverages previous work on equivalent continuum formulation and analytical considerations on the buckling of thin shells. This analytical approach is illustrated by a short parametric study on linear buckling analysis of pseudo-geodesic networks. This study shows that pseudo-geodesic gridshells have the potential to significantly increase the structural performance of gridshells built from straight strips. However, lateral torsional buckling and sensitivity to length variation should be treated with great care in practical applications.

To conclude, some open questions in geometry remain to be solved. First, we used a propagation algorithm to generate pseudo-geodesics. This is also the approach used in [33], but it remains difficult to control the behaviour of pseudo-geodesics and to create regular quadrilateral patterns, especially with high positive Gaussian curvature. Second, it is well-known that asymptotic gridshells can be built on a flat surface and deployed in the fashion of traditional elastic gridshells. Likewise, the spatial deployment of geodesic gridshells is well-understood [39]. However, the spatial deployment of pseudo-geodesic gridshells remains an open question. Finally, by taking a non-constant θ angle, a large potential of innovative structures with high-node congruence remains to

be explored.

References

[1] I. Liddell, Frei otto and the development of gridshells, Case Studies in Structural Engineering 4 (2015) 39–49. doi:https://doi.org/10.1016/j.csse.2015.08.001.
URL https://www.sciencedirect.com/science/article/pii/S2214399815300011

[2] R. Harris, O. Kelly, The structural engineering of the downland gridshell, Space Structures 5 1 (2002) 161.

[3] S. Adriaenssens, M. Barnes, Tensegrity spline beam and grid shell structures, Engineering Structures 23 (1) (2001) 29–36. doi:https://doi.org/10.1016/S0141-0296(00)00019-5.
URL https://www.sciencedirect.com/science/article/pii/S0141029600000195

[4] C. Douthe, O. Baverel, J.-F. Caron, Form-finding of a grid shell in composite materials, Journal of the International Association for Shell and Spatial structures 47 (1) (2006) 53–62.

[5] J. Lienhard, H. Alpermann, C. Gengnagel, J. Knippers, Active bending, a review on structures where bending is used as a self-formation process, International Journal of Space Structures 28 (3-4) (2013) 187–196.

[6] H. Pottmann, M. Eigensatz, A. Vaxman, J. Wallner, Architectural geometry, Computers & graphics 47 (2015) 145–164.

[7] Y. Masson, L. Monasse, Existence of global chebyshev nets on surfaces of absolute gaussian curvature less than 2 pi, Journal of Geometry 108 (1) (2017) 25–32.

[8] C. Douthe, R. Mesnil, H. Orts, O. Baverel, Isoradial meshes: Covering elastic gridshells with planar facets, Automation in Construction 83 (2017) 222–236.

[9] L. D. Peloux, F. Tayeb, B. Lefevre, O. Baverel, J.-F. Caron, Formulation of a 4-dof torsion/bending element for the formfinding of elastic gridshells, in: Proceedings of IASS Annual Symposia, International Association for Shell and Spatial Structures (IASS), 2015.

[10] E. Schling, M. Kilian, H. Wang, J. Schikore, H. Pottmann, Design and construction of curved support structures with repetitive parameters, in: Advances in Architectural Geometry 2018, 2018.

[11] J. Natterer, N. Burger, A. Müller, J. Natterer, Roof of the main hall at expo 2000 in hanover, germany, Structural engineering international 10 (3) (2000) 167–169.

[12] J. Harding, W. Pearson, H. Lewis, S. Melville, The ongreening pavilion, in: Advances in architectural geometry 2014, Springer, 2015, pp. 295–308.

[13] C. Haskell, N. Montagne, C. Douthe, O. Baverel, C. Fivet, Generation of elastic geodesic gridshells with anisotropic cross sections, International Journal of Space Structures 36 (4) (2021) 294–306.

[14] E. Schling, D. Hitrec, R. Barthel, Designing grid structures using asymptotic curve networks, in: Humanizing Digital Reality, Springer, 2018, pp. 125–140.

[15] V. Gioncu, N. Balut, Instability behaviour of single layer reticulated shells, International journal of space structures 7 (4) (1992) 243–252.

[16] S. Nakazawa, S. Kato, T. Takeuchi, S.-D. Xue, C. Lazaro, State-of-the-art of seismic response evaluation methods for metal roof spatial structures, Journal of the International Association for Shell and Spatial Structures 53 (2) (2012) 117–130.

[17] T. Bulenda, J. Knippers, Stability of grid shells, Computers & Structures 79 (12) (2001) 1161–1174.

[18] L. Bruno, M. Sassone, F. Venuti, Effects of the equivalent geometric nodal imperfections on the stability of single layer grid shells, Engineering Structures 112 (2016) 184–199.

[19] B. Lefevre, C. Douthe, O. Baverel, Buckling of elastic gridshells, Journal of the International Association for shell and spatial structures 56 (3) (2015) 153–171.

[20] R. Mesnil, J. Ochsendorf, C. Douthe, Stability of pseudo-funicular elastic grid shells, International Journal of Space Structures 30 (1) (2015) 27–36.

[21] F. Tayeb, J.-F. Caron, O. Baverel, L. Du Peloux, Stability and robustness of a 300 m2 composite gridshell structure, Construction and Building Materials 49 (2013) 926–938.

[22] A. J. Lara-Bocanegra, A. Majano-Majano, J. Ortiz, M. Guaita, Structural analysis and form-finding of triaxial elastic timber gridshells considering interlayer slips: Numerical modelling and full-scale test, Applied Sciences 12 (11) (2022) 5335.

[23] S. Malek, T. Wierzbicki, J. Ochsendorf, Buckling of spherical cap gridshells: A numerical and analytical study revisiting the concept of the equivalent continuum, Engineering Structures 75 (2014) 288–298. doi:https://doi.org/10.1016/j.engstruct.2014.05.049.
URL https://www.sciencedirect.com/science/article/pii/S0141029614003472

[24] R. Mesnil, C. Douthe, O. Baverel, B. Léger, Linear buckling of quadrangular and kagome gridshells: A comparative assessment, Engineering Structures 132 (2017) 337–348. doi:https://doi.org/10.1016/j.engstruct.2016.11.039.

URL https://www.sciencedirect.com/science/article/pii/S0141029616313141

[25] R. Mesnil, C. Douthe, O. Baverel, Non-standard patterns for gridshell structures: fabrication and structural optimization, Journal of the International Association for Shell and Spatial Structures 58 (4) (2017) 277–286.

[26] P. Winslow, S. Pellegrino, S. Sharma, Multi-objective optimization of free-form grid structures, Structural and multidisciplinary optimization 40 (1) (2010) 257–269.

[27] B. D'Amico, A. Kermani, H. Zhang, A. Pugnale, S. Colabella, S. Pone, Timber gridshells: Numerical simulation, design and construction of a full scale structure, Structures 3 (2015) 227–235.

[28] C. Douthe, J.-F. Caron, O. Baverel, Gridshell structures in glass fibre reinforced polymers, Construction and building materials 24 (9) (2010) 1580–1589.

[29] V. Gioncu, Instability problems in space structures, International Journal of Space Structures 1 (3) (1985) 169–183.

[30] F. Venuti, L. Bruno, Influence of in-plane and out-of-plane stiffness on the stability of free-edge gridshells: A parametric analysis, Thin-Walled Structures 131 (2018) 755–768.

[31] F. Venuti, Influence of pattern anisotropy on the structural behaviour of free-edge single-layer gridshells, Curved and Layered Structures 8 (1) (2021) 119–129.

[32] W. Wunderlich, Raumkurven, die pseudogeodätische linien eines zylinders und eines kegels sind, Compositio Mathematica 8 (1951) 169–184.

[33] C. Jiang, K. Mundilova, F. Rist, J. Wallner, H. Pottmann, Curve-pleated structures, ACM Transactions on Graphics (TOG) 38 (6) (2019) 1–13.

[34] R. Mesnil, C. Douthe, O. Baverel, B. Léger, J.-F. Caron, Isogonal moulding surfaces: a family of shapes for high node congruence in free-form structures, Automation in Construction 59 (2015) 38–47.

[35] H. Schober, Transparent shells: Form, topology, structure, John Wiley & Sons, 2015.

[36] R. Mesnil, Stability of elastic grid shells, Ph.D. thesis, Massachusetts Institute of Technology (2013).

[37] S. Pone, S. Colabella, B. D'Amico, A. Fiore, D. Lancia, B. Parenti, Timber post-formed gridshell: Digital form-finding/drawing and building tool, in: Proceedings of IASS Annual Symposia, Vol. 2013, International Association for Shell and Spatial Structures (IASS), 2013, pp. 1–8.

[38] C. Preisinger, M. Heimrath, Karamba—a toolkit for parametric structural design, Structural Engineering International 24 (2) (2014) 217–221.

[39] S. Pillwein, K. Leimer, M. Birsak, P. Musialski, On elastic geodesic grids and their planar to spatial deployment, ACM Transactions on Graphics (TOG) 39 (4) (2020) 125–1.

[40] C. Jiang, K. Mundilova, F. Rist, J. Wallner, H. Pottmann, Curve-pleated structures, ACM Trans. Graph. 38 (6) (nov 2019). doi:10.1145/3355089.3356540.
URL https://doi.org/10.1145/3355089.3356540

Appendix A. Generation of pseudo-geodesic curves

This section presents the method to generate pseudo-geodesic on surfaces. The adopted methodology is similar to the one employed in [40].

Appendix A.1. Pseudo-geodesic from point and tangent vector

It is well-known that it is possible to construct a geodesic on a surface from one point and one arbitrary tangent vector. This property also holds

for pseudo-geodesic curves. Indeed, let us consider a point $\boldsymbol{P}$ on the surface and ϕ the angle between the tangent vector and the first principal curvature direction. It has already established that, for pseudo geodesics with $\theta \neq 0$, we have $\kappa_g = \text{cotan}\theta \cdot \kappa_n$. The normal curvature is known by Euler formula. Furthermore, we can use Bonnet's formula for geodesic curvature:

$$\kappa_g = \frac{d\phi}{ds} \tag{A.1}$$

Where s is the arclength of the curve. The combination of equation (A.1) with Euler's formula yield a first order differential equation in ϕ.

$$\frac{d\phi}{ds} = \text{cotan}\theta \left(\kappa_1 \cos^2\phi + \kappa_2 \sin^2\phi\right) \tag{A.2}$$

This equation rarely has analytical solution. Wunderlich found one for cylinders, where κ_1 is constant and $\kappa_2 = 0$ [32]. We may notice however that when an initial value of ϕ is known, then we may immediately have access to $d\phi/ds$. Thus, an Euler-forward method allows to construct a numerical approximation of the solution when making a small step ε. This method is illustrated in Figure A.22, where $\boldsymbol{e}_1$ and $\boldsymbol{e}_2$ are the first and second principal curvature directions.

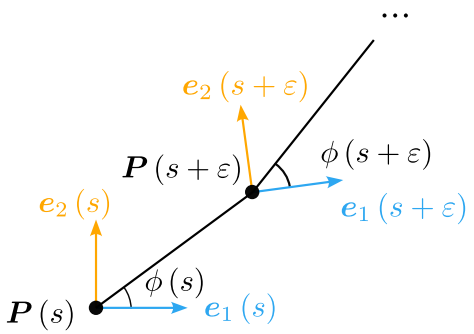

Figure A.22: Iterative generation of a pseudo-geodesic curve.

$$\begin{cases} \phi\,(s+\varepsilon) = \phi\,(s) + \varepsilon\left(\kappa_1 \cos^2\phi + \kappa_2 \sin^2\phi\right) + o\,(\varepsilon) \\ \boldsymbol{P}\,(s+\varepsilon) = \boldsymbol{P}\,(s) + \varepsilon\,(\cos\phi\ \boldsymbol{e}_1 + \sin\phi\ \boldsymbol{e}_2) + o\,(\varepsilon) \end{cases} \tag{A.3}$$

It is possible to iteratively apply this discrete integration scheme, and by doing so, to construct a polyline that converges to the pseudo-geodesic curve when ε

tends to zero. Off course, more sophisticated integration schemes, like Runge-Kutta method may be used to improve accuracy.

Appendix A.2. Implementation

The previous section shows that the iterative construction of a pseudo-geodesic curve from one point and one tangent is possible. However, (A.3) requires to know the principal curvature directions, and may require special care near singularities. For example $-\boldsymbol{e}_1$ is also a principal curvature direction, so the definition of ϕ may be ambiguous when the principal curvature direction evolves rapidly. This is illustrated in Figure A.23.

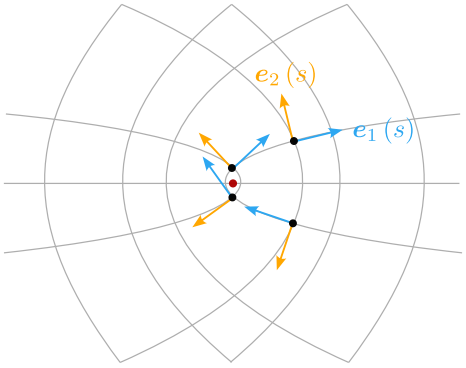

Figure A.23: Principal curvature directions may rapidly change near a lemon-type singularity.

An alternative numerical procedure has thus been implemented in a Grasshopper plug-in. The algorithm also generates a polyline, but doesn't require the computation of principal curvature directions. It is illustrated in Figure A.24 and relies on the very definition of pseudo-geodesics, namely that the angle between the binormal and the surface normal is constant. The algorithm consists in the following steps:

- Estimate tangent vector as $\hat{\boldsymbol{T}}_{n+1} = \boldsymbol{P}_{n+1} - \boldsymbol{P}_n$.
- Retrieve the surface normal $\boldsymbol{n}_{n+1}$.
- Construct $\hat{\boldsymbol{B}}_{n+1}$ by rotating $\boldsymbol{n}_{n+1}$ along $\hat{\boldsymbol{T}}_{n+1}$ with an angle θ.

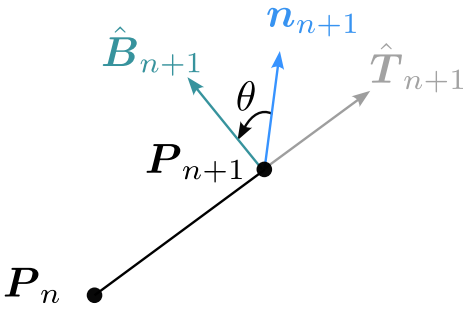

Figure A.24: Determination of the estimation of the curve binormal vector $\hat{\boldsymbol{B}}_{n+1}$ from two previous points $\boldsymbol{P}_n$ and $\boldsymbol{P}_{n+1}$.

- Construct the plane $\mathcal{P}$ of centre $\boldsymbol{P}_{n+1}$ and normal $\hat{\boldsymbol{B}}_{n+1}$.
- Intersect $\mathcal{P}$ with the reference surface, this results in a curve Γ.
- Find a new point $\boldsymbol{P}_{n+2}$ of Γ, for example by intersecting it with a sphere.
- Iterate.